THE JOURNAL OF PHYSICAL CHEMISTRY C
A JOURNAL OF THE AMERICAN CHEMICAL SOCIETY
pubs.acs.org/JPCC
Article

Oxidation of Sn at the Cluster−Support Interface: Sn and Pt−Sn Clusters on $TiO_2(110)$

Sumit Beniwal,[⊥] Wenrui Chai,[⊥] Kamolrat Metavarayuth, Thathsara D. Maddumapatabandi, Deependra M. Shakya, Graeme Henkelman,* and Donna A. Chen*

Cite This: J. Phys. Chem. C 2021, 125, 17671−17683

Read Online

ACCESS | Metrics & More | Article Recommendations | Supporting Information

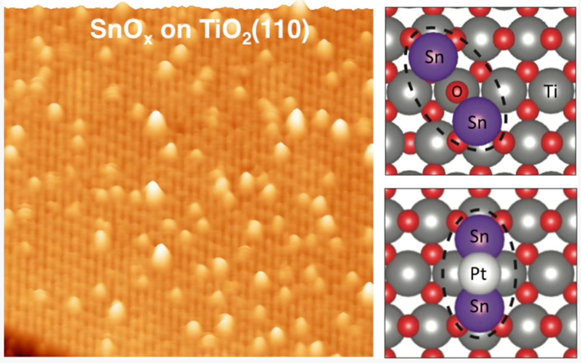

ABSTRACT: The growth of Sn and Pt−Sn clusters on $TiO_2(110)$ has been studied by scanning tunneling microscopy, X-ray photoelectron spectroscopy (XPS), low energy ion scattering (LEIS), and density functional theory (DFT). At low Sn coverages (0.02 ML), single-layer high clusters of SnO_x are formed with a narrow size distribution and uniform spatial distribution. XPS experiments indicate that these clusters consist of oxidized Sn, and the corresponding reduction in the TiO_2 substrate is observed. At higher Sn coverages, the surface is still dominated by two-dimensional clusters of SnO_x, but larger three-dimensional clusters of metallic Sn also appear. As the Sn coverage is increased, the number of three-dimensional clusters increases, and the ratio of Sn/SnO_x increases, suggesting that SnO_x and reduced TiO_x form at the cluster−support interface. When Pt is deposited on top of the Sn/SnO_x clusters, the relatively mobile Pt atoms diffuse across the TiO_2 surface and become incorporated into existing Sn/SnO_x clusters. Furthermore, the addition of Pt to the Sn/SnO_x clusters causes the reduction of SnO_x to metallic Sn and the oxidation of Ti^{3+} to Ti^{4+}; this behavior is attributed to the formation of Pt−Sn alloy clusters, which results in the diffusion of Sn away from the interface with the TiO_2 support. In contrast, when Sn is deposited on an equal coverage of Pt clusters, new Sn/SnO_x clusters are formed that coexist with Pt−Sn clusters. However, the surfaces of both Pt on Sn and Sn on Pt clusters are Sn-rich due to the lower surface free energy of Sn compared to Pt. DFT calculations demonstrate that $M−TiO_2$ bonding is favored over M−M bonding for M = Sn, unlike for transition metals such as M = Pt, Au, Ni, and Co. Furthermore, the substantial charge transfer from Sn to TiO_2 leads to dipole−dipole repulsion of Sn atoms that prevents agglomeration into the larger clusters that are observed for the mid-late transition metals. DFT studies also confirm that the addition of Pt to a Sn cluster results in strong Pt−Sn bond formation and diminished Sn−O interactions.

■ INTRODUCTION

Understanding the Sn/SnO_x interface with titania is a rich area of study due to the importance of this interface in a variety of applications ranging from catalysis[1,2] to gas sensors,[3,4] batteries,[5,6] and electronic devices.[7] Sn^{4+} can be easily substituted for Ti^{4+} in rutile TiO_2, and the resulting materials are believed to possess superior chemical, optical, and electronic properties.[8−15] For applications involving solar cells, doping TiO_2 with Sn^{4+} improves performance by decreasing the band gap.[16] Sn-doped TiO_2 also exhibits excellent photocatalytic activity for reactions such as photodegradation of dyes[17,18] and photo-oxidation of NO_x[19] and organics;[20] this improved photoactivity is attributed to a decrease in the rate of electron−hole recombination and improved light absorption after Sn^{4+} doping.[9,20] For TiO_2 used in the anodes of Li-ion batteries, better power, capacity, and stability are reported after Sn doping.[5,6]

In addition, Sn-containing particles supported on oxides are reported to have unique catalytic activity, particularly when mixed with Pt.[21−24] Specifically, Pt−Sn bimetallic catalysts show superior selectivity compared to pure Pt for hydrogenation of unsaturated aldehydes to the desired unsaturated alcohols.[1,2,25−28] Pt−Sn surfaces are also reported to be more resistant to carbon fouling than pure Pt,[29−31] and the strong interactions between Sn clusters and the oxide support inhibit loss of active sites due to cluster sintering.[2,30] For Pt/TiO_2 and $PtSn/TiO_2$ catalysts used in the selective hydrogenation of unsaturated aldehydes to unsaturated alcohols, interactions between Pt and titania are reported to promote hydrogenation of the C=O bonds over C=C bonds.[1,32−35] Obstacles to establishing fundamental understanding of the chemical

Received: April 14, 2021
Revised: July 6, 2021
Published: August 10, 2021

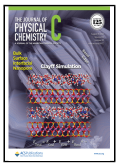

https://doi.org/10.1021/acs.jpcc.1c03338
J. Phys. Chem. C 2021, 125, 17671−17683

processes occurring on Pt−Sn/TiO_2 catalysts are the high sensitivities to: Pt−Sn interactions, alloying; oxidation states; the nature of the support; and the exact catalyst preparation conditions.[1,36−40] Therefore, the rational design of these selective hydrogenation catalysts would significantly benefit from careful control of cluster sizes and compositions, Sn oxidation states, and interactions between the metal cluster and the titania support.

In the work reported here, fundamental investigations of Sn, Pt, and Pt−Sn bimetallic clusters deposited on rutile TiO_2(110) have been carried out by scanning tunneling microscopy (STM), X-ray photoelectron spectroscopy (XPS), and low energy ion scattering (LEIS); the understanding gained from these experiments has been complemented by density functional theory (DFT) investigations. For pure Sn clusters deposited on TiO_2(110), small, uniformly distributed, single-layer clusters are initially formed with SnO_x existing at the cluster−support interface. At higher Sn coverages, the deposited Sn atoms form metallic species in addition to SnO_x at the interface. Exclusively bimetallic Pt−Sn clusters are prepared by deposition of Pt on top of existing Sn clusters, and the surfaces of these clusters are found to be Sn-rich, indicating facile diffusion of Sn atoms within the clusters. Incorporation of Pt into the Sn clusters results in the loss of SnO_x as Sn diffuses away from the metal−TiO_2 interface in order to form the energetically favored Pt−Sn bonds. DFT studies confirm that Sn−Sn interactions are weaker than the Sn−TiO_2 interactions due to charge transfer to TiO_2 and dipole−dipole repulsion between Sn atoms, which prevents agglomeration into the larger clusters observed for transition metals such as Pt, Au, Ni, and Co.

■ METHODS

Experimental Methods. Experiments were carried out in two ultrahigh vacuum chambers that have been described in detail elsewhere. The first chamber has a base pressure of 1×10^{-10} Torr[41,42] and is equipped with a variable-temperature scanning tunneling microscope (Omicron VT-25), a single-channel hemispherical analyzer (Omicron EA125) for XPS and LEIS spectroscopy, optics for low energy electron diffraction (LEED) and Auger electron spectroscopy (AES, Omicron Spec 3), a quadrupole mass spectrometer (Leybold-Inficon, Transpector 2), and a load lock chamber for rapid introduction of samples and STM tips. The second chamber[43,44] has a base pressure of 1×10^{-9} Torr and houses a multichannel hemispherical analyzer (Omicron EA2000 SPHERA) for XPS studies, a custom-designed microreactor, a quadrupole mass spectrometer (Stanford Research Systems, RGA 300), and a load lock chamber. The second chamber was used only for the low coverage 0.02 monolayer (ML) Sn XPS experiment, which required the higher sensitivity XPS analyzer.

The rutile TiO_2(110) crystal (Princeton Scientific Corporation, 10 mm × 10 mm × 1 mm) was mounted onto a standard Omicron Ta sample plate as previously described.[45] Sample heating was carried out by electron bombardment of the Ta back plate that was directly in contact with the crystal,[45] and sample temperatures were measured using a calibrated infrared pyrometer (Heitronics).[45,46] The TiO_2(110) crystal was cleaned by multiple cycles of Ar^+ ion sputtering at 1 kV for 20 min and annealing to 950−1000 K for 3 min; sample cleanliness and order were confirmed by a combination of STM, XPS, and LEED.

Metal clusters of Pt and Sn were prepared by vapor deposition from a Pt rod (ESPI, 2 mm diameter, 99.95%) and Sn pellets (ESPI, 99.999%) housed in a tungsten crucible using a four-pocket electron-beam evaporator (Oxford Applied Research, EGCO4). The deposition rates were 0.020−0.025 ML/min for Pt and 0.035 ML/min for Sn. Before each metal deposition, the flux was measured with a quartz crystal microbalance (QCM, InficonXTM-2). The QCM was independently calibrated by depositing submonolayer, single-layer islands of Sn on Pt(111) and Pt on Pt(111) at room temperature and measuring the fraction of the surface covered by the islands in the STM images.[47] For both Pt and Sn, one ML is defined as the packing density of the Pt(111) surface ($1 \text{ ML} = 1.50 \times 10^{15}$ atoms/cm^2).

STM imaging was carried out at room temperature at sample bias voltages of +1.4−2.3 V with respect to the tip and constant tunneling currents of 10−100 pA. The STM tips consisted of electrochemically etched tungsten wire (0.38 mm diameter) and were conditioned by Ar^+ sputtering and voltage pulsing (up to +10 V) on clean substrates. Cluster heights were determined using an automated in-house program,[48,49] which measured all clusters in a 110 × 110 nm^2 image (900−2700 clusters). The errors reported with the cluster heights are the standard deviations. Cluster densities were determined by manually counting all clusters in a 110 × 110 nm^2 region to avoid potential problems with the automated program undercounting the smallest clusters in cases where there is a large range of cluster heights. Since cluster diameters are known to be overestimated due to tip convolution effects,[50,51] average cluster heights are reported as a measure of cluster size. Image flattening and deglitching were carried out with the WSXM shareware program.[52] Average cluster sizes in atoms/clusters were estimated for the 0.02 ML Sn and 0.05 ML Pt surfaces by dividing the total number of atoms deposited per cm^2, as measured using the QCM, by the number of clusters in given area. Estimates of atoms/clusters were not made for the other surfaces because the size distributions were broad, and large clusters coexisted with small ones on the surfaces with higher Sn coverages.

XPS experiments were carried out with an Al Kα X-ray source in the first chamber and a Mg Kα source in the second chamber. The XPS data for the Ti(2p), O(1s), Pt(4f), and Sn(3d) regions were collected with a pass energy of 50 eV, a step size of 0.020 eV, and dwell times of 0.2, 0.3, 0.2, and 0.3 s, respectively. Casa XPS 2.3.16 software with a Shirley-type background was used for peak fitting.[53] Ti(2p), Sn(3d), and O(1s) peaks were fit with Gaussian−Lorentzian (GL) line shapes with values for a full width at half-maximum (fwhm) of 1.7−1.8, 1.9−2.2, and 1.5−1.7 eV, respectively. These parameters are consistent with values in the literature and data previously collected with this XPS system.[42] Based on previously published work, Sn($3d_{5/2}$) spectra were fit with two GL peaks with fwhms of 1.9−2.2 eV[19,54−56] and O(1s) spectra were fit by two GL components with fwhms of 1.5−1.7 eV.[57−59]

LEIS experiments were conducted with 600 eV He^+ ions, and collection parameters were chosen to minimize beam damage during data collection. Specifically, a 25 μA current to the sample for Pt−Sn/TiO_2 surfaces resulted in a less than 10% loss in the Pt signal and no loss in the Sn signal for successive scans at a step size of 0.2 eV and a dwell time of 0.1 s. For the purpose of deconvoluting the Pt and Sn peaks to

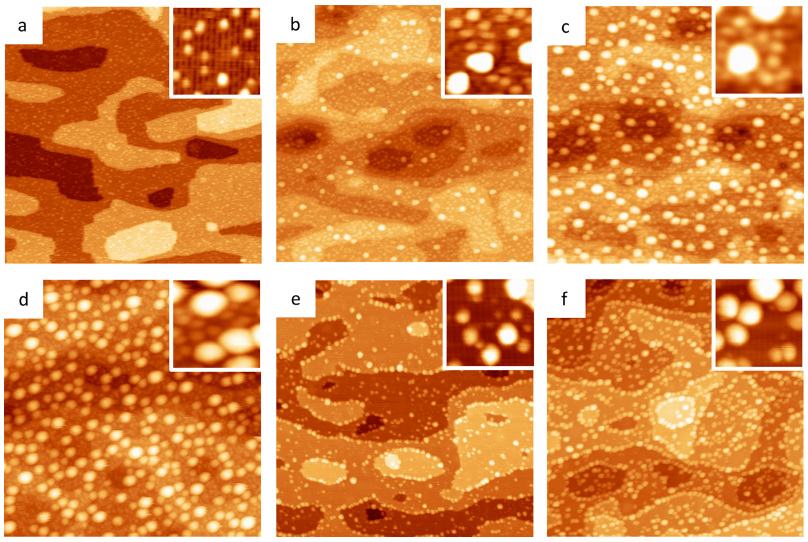

Figure 1. STM images for (a) 0.02 ML Sn; (b) 0.05 ML Sn; (c) 0.13 ML Sn; (d) 0.25 ML Sn; (e) 0.05 ML Pt; and (f) 0.13 ML Pt on $TiO_2(110)$. Images are 110 × 110 nm^2, and insets are 10 × 10 nm^2.

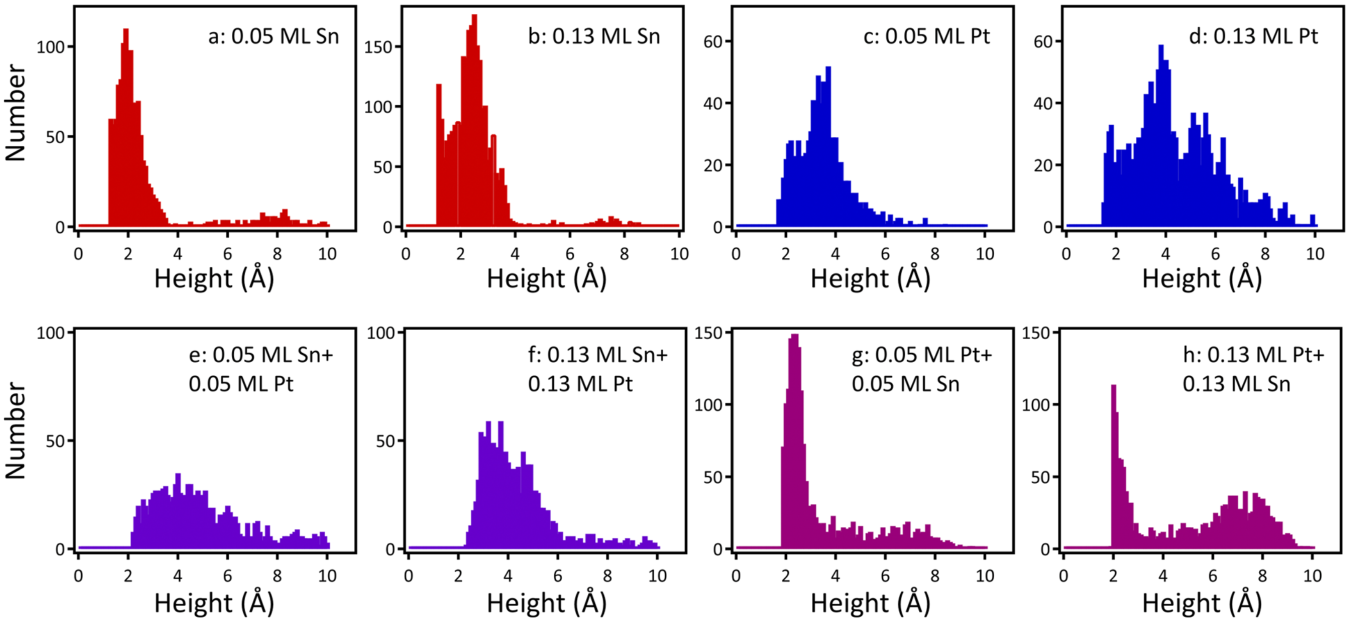

Figure 2. Cluster height histograms for pure (top) and bimetallic (bottom) clusters on $TiO_2(110)$.

measure the areas, the LEIS spectra were fit with Gaussian peaks using the automated fitting software in Igor Pro 6.2.

Computational Methods. DFT calculations were conducted with the Vienna Ab Initio Software Package.[60−63] Core electrons were described within the projected augmented wave framework,[64] and valence electrons were described with a plane-wave basis set up to an energy cutoff of 400 eV. The generalized gradient approximation in the form of the Perdew, Burke, and Ernzerhof functional was used to describe electronic exchange and correlation.[65] While DFT + *U* is important to describe localized electrons on the Ti atoms in the surface, it was not important for our calculated binding energies. Specifically, the binding energies of Au and Sn differ by only 0.013 and 0.014 eV, respectively, with the addition of +*U*.

The TiO_2 slab used in this study was a supercell of a (10 × 3 × 3) rutile (110) unit cell with 12 Å of vacuum, and the resulting slab is 29.68 × 19.8 Å. At 0.068 ML coverage, the separation distance was 7.03 Å for isolated Sn_2O clusters, 6.66 Å for isolated adatoms, and about 16 Å for metal clusters. One layer of TiO_2 atoms at the bottom of the slab was constrained in the bulk positions, while all other atoms were relaxed. The box size was chosen to provide sufficient spacing between periodic images and to accurately represent the experimental coverages. The Brillouin zone was sampled at the Γ point, which was found to be sufficient for the large cell modeled here. Additional details about the supported cluster models can be found in Supporting Information.

Binding energies are calculated using eq 1, where E_{binding} is the binding energy of clusters or adatoms, E_{sys} is the energy of the TiO_2 surface with adsorbed clusters or adatoms, n is the number of adsorbed metal atoms present, E_{metal} is the atomic cohesive energy of the corresponding bulk metal, and E_{TiO_2} is the energy of the clean TiO_2 surface.

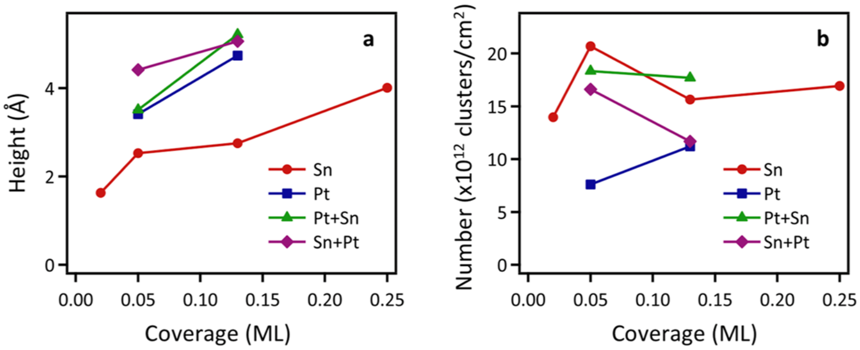

Figure 3. Average cluster height and cluster density as a function of Sn or Pt coverage. For the bimetallic clusters, the value on the *x*-axis represents the coverage of each metal, not the total coverage.

$$E_{\text{binding}} = E_{\text{sys}} - n \times E_{\text{metal}} - E_{\text{TiO}_2} \tag{1}$$

The electric dipole potential is calculated using eq 2 where r is the separation between the center of mass of positive and negative charges and μ_1 and μ_2 are the dipole moments of the positive charge and the summed dipole moments of negative charges, respectively. All surface dipoles were oriented parallel to each other.

$$V_{\text{dipole}} = -\frac{2\mu_1\mu_2}{4\pi\varepsilon_0 r^3} \tag{2}$$

■ RESULTS

STM Studies. STM experiments show that the deposition of 0.02 ML of Sn results in many small clusters with an average cluster height of 1.6 ± 0.3 Å, which corresponds to single-layer clusters (Figure 1a); since the size distribution is narrow (Figure S1a), the average size of these clusters can be estimated as 2 atoms, based on the total number of metal atoms deposited divided by the number of clusters on the surface. Furthermore, the clusters are uniformly distributed over the surface with no preference for adsorption at the energetically favorable step edges, implying that the diffusion length of the Sn atoms is significantly shorter than the width of the terraces. When the Sn coverage is increased to 0.05 ML, the height distribution becomes broader due to the contribution of multilayer clusters, as shown in the histograms in Figure 2. The average cluster height increases to 2.5 ± 1.2 Å, and larger clusters ranging from 6 to 9 Å in height are observed in addition to the single-layer clusters. As the coverage is increased to 0.13 and 0.25 ML, the number of large clusters 6–10 Å in height continues to increase (Figures 1c,d, 2b and S1b). Although these larger clusters are prominent in the STM images of the 0.05–0.25 ML Sn surfaces, the number of clusters larger than 7 Å represents only a small fraction of the total clusters: 5% at 0.05 ML, 8% at 0.13 ML, and 10% at 0.25 ML. Plots of cluster height and cluster density versus coverage are presented in Figure 3. The average cluster height grows with increasing Sn coverage, as shown in Figure 3a. There is initially a significant increase in the number of clusters on the surface (cluster density) from 0.02 to 0.05 ML, but the cluster densities at 0.13 and 0.25 ML are only slightly higher than those at 0.02 ML (Figure 3b). This could be due in part to cluster coalescence at the higher coverages; however, it should be noted that the coexistence of the large clusters with the monolayer clusters for the 0.13–0.25 ML Sn coverages causes the surfaces to be difficult to image with high resolution, and therefore, it is possible that the smaller clusters are undercounted.

Pt growth was also studied on $TiO_2(110)$ for comparison to Sn growth at the same coverages (Figure 1e,f). For 0.05 ML of Pt, the average cluster height is substantially larger (3.4 ± 1.1 Å), and the average number of atoms/cluster is estimated to be ∼10. The preference for the Pt clusters to reside at the step edges suggests higher mobility of Pt atoms on the surface compared with Sn. Furthermore, the number of clusters on the surface is only ∼40% that of 0.05 ML Sn (Figure 3b), and the cluster size distribution is broader for Pt. Although there are fewer clusters larger than 7 Å in height for Pt, there are more Pt clusters in the intermediate size range of 4–6 Å (Figures 1e, 2c). The same is true for the comparison of 0.13 ML Pt with 0.13 ML Sn: in the case of Pt (Figure 1f), the number of clusters is lower (Figure 3b), the average cluster height is greater (4.7 ± 1.5 Å for Pt versus 2.7 ± 2.0 Å for Sn, Figure 3a), and the size distribution is much broader with many more clusters in the range of 4–6 Å (Figure 2d). Between 0.05 and 0.13 ML, the cluster density increases by 50%, and the clusters occupy a large fraction of the step sites at the higher coverage.

Bimetallic Pt–Sn surfaces were prepared by sequential deposition of equal coverages of the two metals. When 0.05 ML Pt is deposited on 0.05 ML Sn (Sn + Pt), the number of clusters does not increase, but the cluster heights increase, resulting in a significant broadening of the size distribution (Figures 4a, 2a,e, and 3). This behavior indicates that all of the incoming Pt atoms join the existing Sn clusters, and exclusively bimetallic clusters are formed. For the reverse order of deposition of 0.05 ML Sn on 0.05 ML Pt (Pt + Sn), many small Sn clusters appear at new nucleation sites in addition to an increase in the average height of the existing Pt clusters (Figures 4b, 2c,g, and 3). The increase in the number of clusters is consistent with the lower mobility of Sn that does not allow the Sn atoms to diffuse to the existing Pt clusters, and therefore, the surface consists of both pure Sn clusters and Pt–Sn clusters. Consequently, the size distribution is bimodal because it includes the new small Sn islands and the larger bimetallic clusters consisting of Sn on Pt (Figure 2g). These same effects are also observed for the higher-coverage surfaces with 0.13 ML Pt and 0.13 ML Sn. In the case of 0.13 ML Sn + 0.13 ML Pt (Figure 4c), the initial high density of small Sn clusters serves as nucleation sites for the deposited Pt atoms, and the number of clusters on the surface does not increase after the deposition of Pt (Figure 3b). Pt is incorporated into the Sn existing clusters, as illustrated by the increase in height from 2.7 ± 2.0 to 5.1 ± 2.1 Å after Pt deposition (Figure 3a).

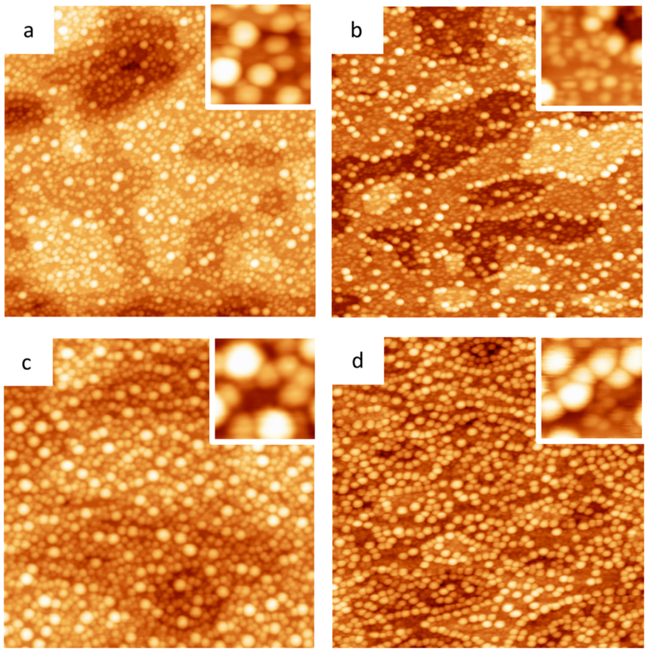

Figure 4. STM images for (a) 0.05 ML Sn + 0.05 ML Pt; (b) 0.05 ML Pt + 0.05 ML Sn; (c) 0.13 ML Sn + 0.13 ML Pt; and (d) 0.13 ML Pt + 0.13 ML Sn on $TiO_2(110)$. Images are 110 × 110 nm^2, and insets are 10 × 10 nm^2.

In the case of 0.13 ML Pt + 0.13 ML Sn, the initial deposition of the more mobile Pt atoms results in a low cluster density with clusters that preferentially nucleate at the step edges (Figure 1f). The subsequent deposition of Sn causes both a minor increase in height from 4.7 ± 1.5 to 5.2 ± 2.4 Å and the formation of many small Sn clusters in the regions between the Pt clusters (Figures 3, 4d). Bimodal distributions are clearly observed for both Sn on Pt surfaces that reflect contributions from the small Sn clusters and from the larger bimetallic clusters formed via Sn incorporation into the existing Pt clusters (Figure 2g,h).

LEIS Studies. The surface compositions of the bimetallic surfaces were probed by LEIS, which samples the composition of only the top monolayer. The integrated area of the Pt peak for 0.13 ML Pt clusters decreases to 18% of its initial value after deposition of 0.13 ML Sn, indicating that the majority of the Pt surface is covered after Sn deposition (Figure 5). The enrichment of Sn at the surface is consistent with the lower surface free energy of Sn compared with Pt (0.51[66] versus 2.5 J/m^2[67]), but the surfaces of these clusters are richer in Sn than what would be expected for the PtSn and Pt_3Sn alloys commonly observed in PtSn nanoparticles.[68,69] In contrast, the Sn signal decreases by only ~15% after deposition of 0.13 ML Pt on 0.13 ML Sn, and the Pt signal for the bimetallic surface is ~55% of that for the 0.13 ML Pt clusters. For this surface, the dispersion of metal atoms is higher than that for pure 0.13 ML Pt because Pt atoms nucleate at the many Sn/SnO_x clusters that initially exist on the surface. However, the overall Pt signal is approximately half of that for pure 0.13 ML Pt, which implies that fewer Pt atoms reside at the cluster surface. Thus, the LEIS results demonstrate that the cluster surfaces are Sn-rich even when Pt is deposited on top of Sn, and this behavior is explained by facile diffusion of the metal atoms within the clusters at room temperature, as has been previously observed for other bimetallic clusters on $TiO_2(110)$, such as Pt−Au[70] and Ni−Au.[48]

XPS Studies. XPS investigations indicate that Sn is oxidized when deposited directly on TiO_2. These experiments were carried out with the sample at a grazing angle (72°) with respect to the detector in order to enhance surface sensitivity. The 0.02 ML Sn/TiO_2 surface, which consists of only single-layer clusters, exhibits a single $Sn(3d_{5/2})$ peak at 487.1 eV attributed to SnO_x (Figure 6). For a higher coverage of 0.05 ML Sn, peaks for both metallic Sn at 484.8 eV and SnO_x at 487.3 eV are observed with roughly equal intensities. The 484.8 eV binding energy is in agreement with the 484.5−485.2

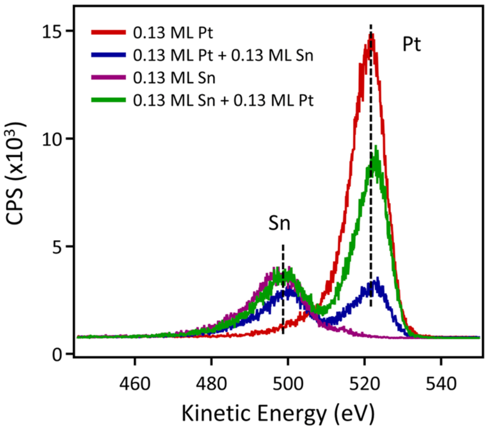

Figure 5. LEIS data for Pt, Sn, and Pt−Sn clusters on $TiO_2(110)$.

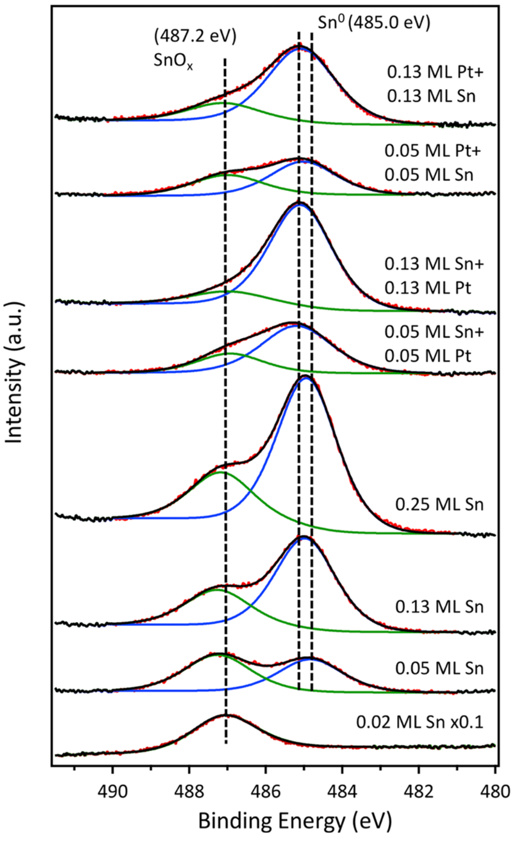

Figure 6. XPS data for the $Sn(3d_{5/2})$ region for metal clusters on $TiO_2(110)$. The 0.02 ML spectrum was acquired with the multichannel analyzer.

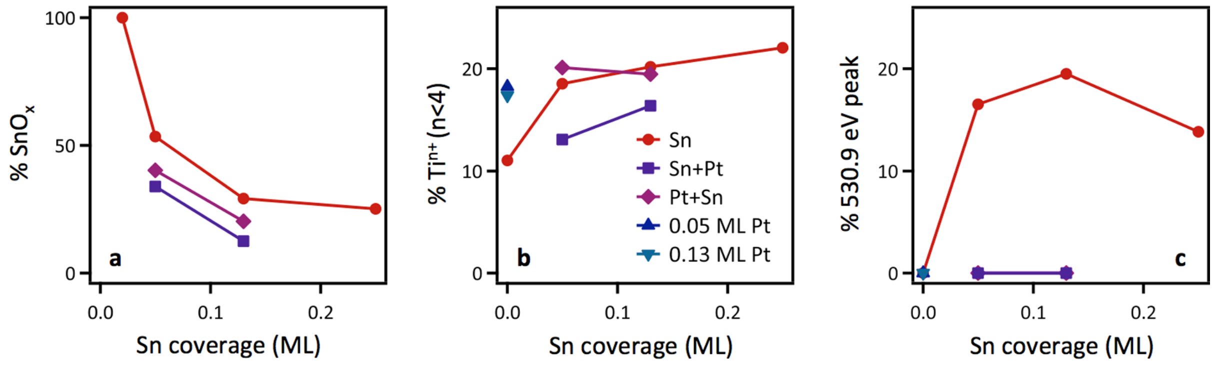

Figure 7. Following properties determined from XPS data as a function of Sn coverage for pure clusters and Pt–Sn clusters: (a) % SnO_x; (b) % Ti^{n+} ($n < 4$); and (c) % contribution of the 530.9 eV peak to the total O(1s) signal. For the Pt + Sn and Sn + Pt surfaces, the Pt coverage is always equal to the Sn coverage.

eV values reported for metallic Sn.[24,71−75] The value of 487.3 eV is higher than the ~486.0−486.6 eV[4,19,76,77] assigned to Sn^{4+} in bulk SnO_2, but clusters[24,54,68,74,78] and thin films[18,79] generally have higher binding energies than bulk SnO_2 and have been observed at ~487 eV. Given the similarities between the Sn^{2+} and Sn^{4+} binding energies in oxides, especially in cases where the structure of SnO_x is not well-defined, it is difficult to distinguish between SnO_2 and SnO.[19,72,73,75−77] Due to the small signals that we observe for the low Sn coverages, the use of the Auger parameter[72,80] is also not a reliable method of distinction between SnO and SnO_2.

As the coverage is increased to 0.13 ML, there is no change in the SnO_x peak intensity, whereas the metallic feature grows. This suggests that the larger clusters observed in the STM images are metallic Sn, while the smaller clusters correspond to SnO_x. At 0.25 ML Sn, the metallic Sn peak continues to grow, and there is also a smaller increase in the SnO_x peak. Figure 7a illustrates that the fraction of oxidized Sn decreases with increasing Sn coverage, and we propose that SnO_x is formed at the interface between the Sn clusters and the TiO_2 substrate. With increasing Sn coverage, the total Sn−TiO_2 interface increases, but the fraction of Sn atoms at the interface decreases.

In the case of the bimetallic Pt−Sn surfaces, incorporation of Pt into the existing Sn clusters results in an increase in metallic Sn at the expense of SnO_x. When 0.05 ML Pt is deposited on top of 0.05 ML Sn to form bimetallic clusters, the intensity of the SnO_x peak diminishes, and the metallic Sn peak shifts to 485.1 eV (Figure 6). This shift to higher binding energy is attributed to the formation of a Sn−Pt alloy, given that the metallic Sn($3d_{5/2}$) binding energy is 0.3−0.6 eV higher in Pt−Sn alloy nanoparticles;[24,81] a similar shift of +0.2−0.3 eV is observed for Sn alloyed into Pt(111) surfaces.[76,82,83] The loss of the SnO_x peak is ascribed to the diffusion of Sn away from the interface with TiO_2 and into the interior of the cluster in order to increase the favorable interactions between Pt and Sn atoms.[84] The relatively large heat of formation (30−80 kJ/mol) for intermetallic PtSn compounds favors alloying over the monometallic phases.[85−87] Similarly, the deposition of 0.13 ML Pt on 0.13 ML Sn causes a decrease in the SnO_x intensity and a smaller shift in the Sn($3d_{5/2}$) binding energy of +0.1 eV. For both the low and high coverage surfaces, the Sn($3d_{5/2}$) binding energy of SnO_x also shifts by −0.3 eV after Pt deposition and could be related to disruption of the SnO_x phases following the addition of Pt atoms. For Pt deposited on Sn, a smaller fraction of Sn atoms is oxidized compared to the same coverages of Sn on Pt (Figures 6 and 7a). This behavior is explained by a lower percentage of Sn existing in bimetallic clusters for Sn on Pt, given that the Sn atoms form new Sn clusters rather than being incorporated into the Pt clusters. The Pt(4f) spectra for pure Pt and Sn on Pt ($\theta_{Pt,Sn}$ = 0.05 and 0.13 ML) show that there is a small 0.2 eV shift to higher binding energy after Sn deposition on the Pt clusters for both coverages (Figure S2). Since the surface of the clusters is expected to be Sn-rich based on the lower surface free energy of Sn compared to Pt, the shift in the Pt(4f) peaks could be attributed in part to a surface core level shift due to the loss of the low binding energy, undercoordinated Pt atoms at the surface.[88,89] However, a positive shift (~+0.3 eV) in Pt($4f_{7/2}$) binding energy is also consistent with Pt−Sn alloying,[24,25,68,77,85,90−92] which is expected to occur, given the ability of Pt−Sn systems to alloy over a wide range of compositions.[87]

There is also evidence that the TiO_2 substrate is being reduced by Sn deposition based on the appearance of Ti^{n+} ($n < 4$) species. The clean TiO_2 surface has a small percentage of Ti^{3+} due to the preferential removal of oxygen from the crystal during the sputtering and annealing process (Figure 8).[93−95] Before Sn deposition, the Ti^{3+} content for this crystal is 11%, and after deposition of 0.05−0.13 ML Sn, the amount of Ti^{3+} increases to 19−20%, whereas the 0.25 ML Sn exhibits 18% Ti^{3+} and 4% Ti^{2+} (Figures 7b and 8). For Pt on Sn surfaces, where the addition of Pt to the Sn clusters causes Sn to diffuse away from the cluster−TiO_2 interface, the percentage of Ti^{3+} decreases after the addition of 0.05 ML and 0.13 ML Pt to 13 and 16%, respectively (Figures 7b and 8). In the case of Sn deposited on Pt clusters, the percentage of reduced Ti^{n+} is greater than the equivalent coverages of Pt on Sn because there is a significant number of Sn atoms that form pure clusters on TiO_2 rather than nucleating at Pt clusters (Figures 7b and S3). Although the fraction of reduced Ti^{n+} for Sn on Pt (~20%) appears to be comparable to that of pure Sn in Figure 7b, it should be noted that the Sn on Pt experiments were carried out on the TiO_2 substrate after multiple Sn depositions followed by cleaning by sputtering and annealing, which increased the Ti^{3+} content to ~20% for clean TiO_2 without any deposited metal; the same is true for the pure Pt on TiO_2 experiments in Figure 7b. Sn deposition, particularly at the higher coverages of 0.13 ML, increased the rate at which that clean TiO_2 was reduced, most likely because multiple sputtering annealing cycles (~15) were required to remove residual Sn after each experiment.

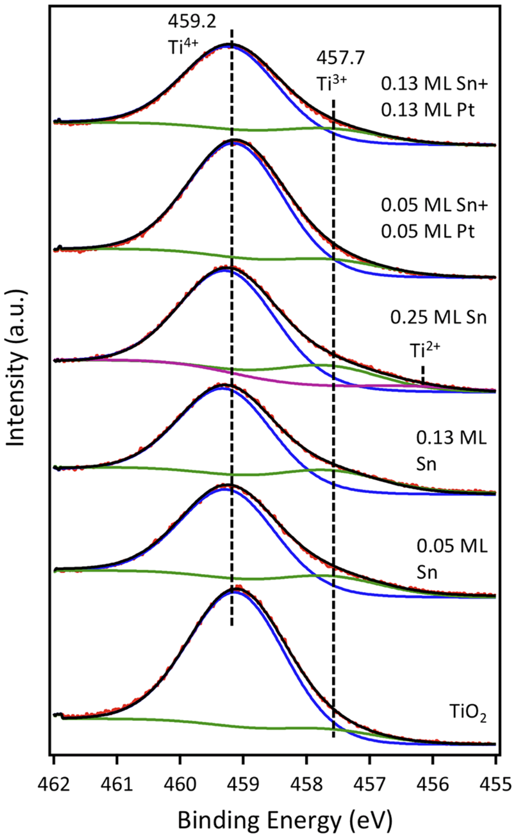

Figure 8. XPS data for the Ti($2p_{3/2}$) region for metal clusters on $TiO_2(110)$.

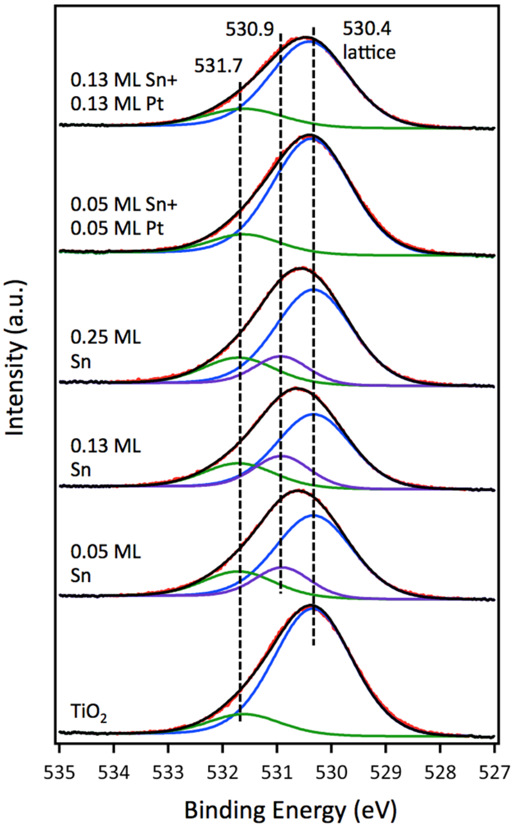

Figure 9. XPS data for the O(1s) region for Sn and Sn + Pt clusters on $TiO_2(110)$.

The O (1s) region confirms the presence of strong Sn−O interactions for pure Sn deposited on TiO_2. For the clean TiO_2 surface, the lattice oxygen peak is observed at 530.4 eV, and there is also a small shoulder that appears at 531.6−531.7 eV, which is assigned to undercoordinated oxygen atoms at the surface (Figure 9).[57,96] When Sn is deposited on the surface, the O(1s) peak shifts to higher binding energy due to the appearance of a peak at 530.9 eV (Figure 9). The contribution of the 530.9 eV peak to the total O(1s) signal is ∼15% at 0.05 ML Sn and does change significantly for Sn coverages of 0.13 and 0.25 ML (Figure 7c). However, when Pt is deposited on the Sn clusters, the 530.9 eV peak ascribed to the Sn−O interactions disappears, and the O(1s) peak shape is the same as that on clean TiO_2 (Figures 9 and 7c). Notably, the 530.9 eV feature is not observed in the O(1s) spectra for pure Pt clusters or Sn on Pt clusters (Figures 7c and S4), which have an O(1s) peak shape identical to that of clean TiO_2. The O(1s) binding energy of 530.9 eV is in the range of what has been reported for SnO_x (530.4−531.4 eV)[79,97,98] but is higher than the binding energies for oxygen in $Sn_xTi_{1-x}O_y$ (529.6−530.2).[9,99]

DFT Calculations. DFT calculations were carried out to help understand the qualitative difference between the observed high density of Sn clusters that are formed on the TiO_2 surface as compared to transition metals, such as Pt, Au, Ni, and Co. A key reason can be seen directly from the calculated structures of the lowest energy clusters of these metals on TiO_2. Figure 10a shows that the most stable clusters of Au on TiO_2 clearly favor Au−Au bonding in three-dimensional clusters; similar structures were found for Ni and Pt. Co also favors clustering, but these clusters are more two-dimensional and can incorporate oxygen from the TiO_2 lattice (Figure 10b). In contrast, Sn atoms repel each other on the TiO_2 surface so that the most stable Sn structures at low coverages are isolated adatoms, as shown in Figure 10c. Consequently, the dispersion of Sn atoms on the TiO_2 surface and the high density for nucleation sites are thermodynamically preferred, whereas Pt, Au, Ni, and Co atoms prefer to aggregate into larger clusters. The energies calculated for all cluster configurations are shown in Tables S1 and S2, and a description of how those configurations were found is provided in the Supporting Information.

DFT calculations provide a compelling explanation of why Sn exhibits qualitatively different behavior from the transition metals in terms of preference for M−TiO_2 bonding over M−M bonding (M = deposited metal). There are two important differences between Sn and the transition metals in terms of their interactions with the TiO_2 surface. First, as shown in Figure 11a, the binding of Sn adatoms to TiO_2 at low density is stronger (more negative) as compared to bulk Sn, whereas the transition metals have stronger M−M bonds than M−TiO_2 bonds (positive binding energies) and therefore favor clustering on the surface. The second difference in the M−TiO_2 interaction is the extent of charge transfer between the metals and the TiO_2 surface determined by a Bader charge analysis.[100−102] Specifically, Sn transfers a charge of 1.3 e to the TiO_2 surface, while Au and Pt transfer charges of 0.45 and 0.50 e, respectively. The charge transfer between adatoms and the oxide surface creates repulsive dipoles. Although this repulsion exists for both Sn and the transition metals, the larger repulsion for Sn combined with the weaker Sn−Sn bonds favor isolated

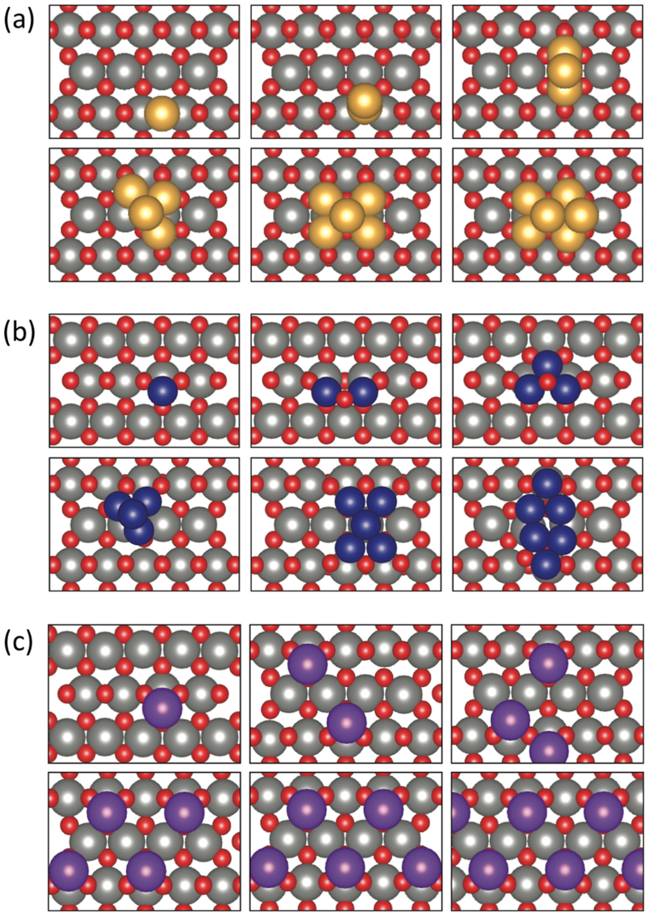

Figure 10. (a) Lowest energy clusters for Au on TiO_2 are three-dimensional, and similar structures were found for Ni and Pt; (b) greater number of two-dimensional clusters were found for Co on TiO_2; and (c) lowest energy structures of Sn on TiO_2. In contrast to Au, Ni, Pt, and Co, Sn atoms repel each other and prefer to remain isolated on the TiO_2 surface.

Sn atoms, whereas the weaker dipole repulsion for the transition metals and the stronger M−M bonds for the transition metals favor the formation of larger clusters. This also explains the larger increase in binding energy per adatom with increasing metal coverage for Sn compared with the other metals (Figure 11a). The qualitative difference in dipole repulsion between Sn adatoms and that of the other metals is shown in Figure 11b, which compares the repulsions calculated from DFT with the dipole repulsions of different densities of isolated atoms on the TiO_2 surface based on a simple sum of dipole−dipole interactions. The DFT calculation is the difference between total binding energy for all of the isolated atoms on the surface and the binding energy of a single isolated atom multiplied by the total number of atoms. The trend for Sn along the $x = y$ dashed line indicates that the dipole−dipole interactions dominate the adatom interaction. However, for the transition metals, dipole−dipole interactions are weaker, and other factors are clearly important for their interaction energies.

DFT calculations also provide insights into the formation of SnO_x for Sn and PtSn clusters. When the Sn coverage is high enough such that clustering of Sn cannot be avoided, two Sn atoms in a cluster will incorporate an O atom from the TiO_2 surface to form a particularly stable Sn_2O unit (Figure 12a),

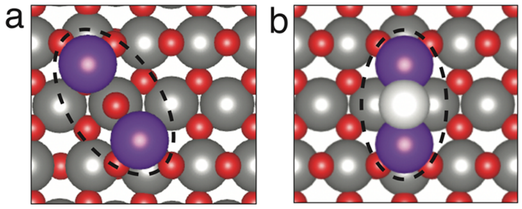

Figure 12. (a) Two Sn atoms brought together spontaneously form a stable Sn_2O cluster incorporating an O atom from the TiO_2 surface and (b) upon the addition of a Pt atom to the Sn_2O cluster, a reduced Sn_2Pt cluster becomes more stable, returning the O atom to the titania surface.

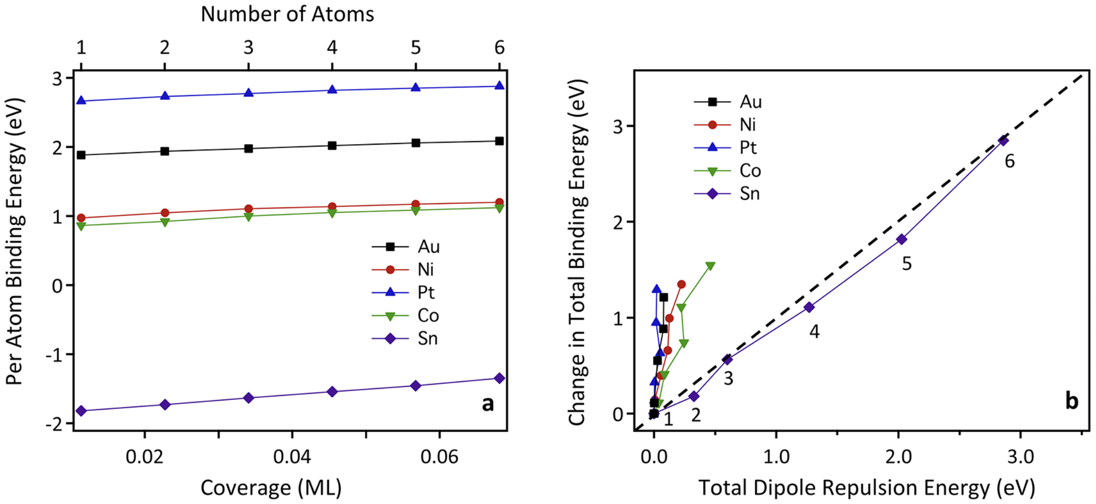

Figure 11. (a) Per atom binding energy of adatoms on the TiO_2 surface as a function of coverage. The positive slopes indicate repulsion between the adatoms, and the negative values for Sn indicate that isolated atoms are favored over bulk Sn; (b) correlation between the repulsive energy of adatoms on the TiO_2 surface calculated using a dipole−dipole interaction (*x*-axis) and from DFT (*y*-axis). The trends are a function of the number of atoms on the surface (indicated for Sn) corresponding to the adatom densities shown in (a).

similar to how Co clusters of size 2 and 3 can reduce the surface (Figure 10b). When comparing stability of this arrangement with other forms of Sn on the surface, we can see that isolated Sn_2O clusters are the most stable at all coverages (Figure 13). Thus, the Sn_2O clusters will be present up to the coverages at which larger clusters must form. This result agrees with the experimental Sn cluster size of two atoms for low coverages and with the XPS studies indicating that small Sn clusters are oxidized on the TiO_2 surface. Additionally, when a Pt atom is added to the cluster (Figure 12b), the Pt atom forms strong bonds with Sn, which becomes reduced to the metallic state. Again, this is consistent with experimental observations that deposition of Pt on Sn/SnO_x clusters on TiO_2 results in metallic PtSn clusters.

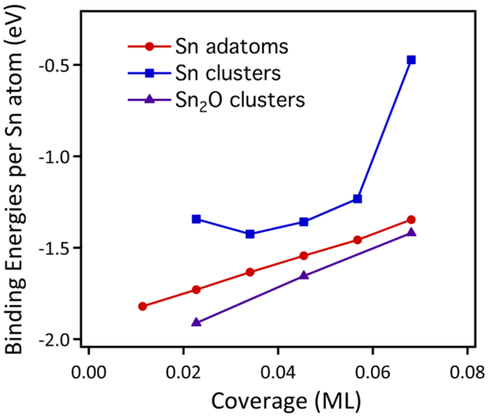

Figure 13. Binding energies per Sn atom as a function of Sn coverage for isolated Sn adatoms, single Sn clusters, and Sn_2O clusters.

■ DISCUSSION

The initial growth of Sn on $TiO_2(110)$ occurs through the formation of small (~2 Sn atoms) clusters that are uniformly dispersed over the surface. XPS studies indicate that Sn exists exclusively as SnO_x rather than metallic Sn at a low coverage of 0.02 ML. At higher coverages, larger multilayer clusters are formed, and metallic Sn coexists with SnO_x. Furthermore, the increase in Ti^{3+} and Ti^{2+} species after Sn deposition shows that the titania support is reduced as Sn is oxidized. The oxidation of Sn and reduction of titania are believed to occur at the cluster−support interface, given that the fraction of Sn existing as SnO_x decreases with increasing Sn deposition for coverages at which most of the surface appears to already be covered by Sn clusters; similarly, there is little increase in the fraction of reduced titania above Sn coverages of 0.05 ML. Other studies of Sn layers deposited on TiO_2 have also shown that Sn grows as an oxide in the first layer.[103] As the Sn coverage is increased, an increasing number of larger (>7 Å high) clusters are observed. Based on XPS data, these larger clusters are believed to consist primarily of metallic Sn, and it is proposed that the diffusion of Sn atoms occurs more readily after the majority of the surface is covered by SnO_x islands.

The growth of Sn on $TiO_2(110)$ is qualitatively different from that of many other metals studied by STM on $TiO_2(110)$, including Pt,[70,104,105] Ni,[106] Au,[70,104,107,108] Pd,[109] Cu,[106,110] Ag,[111] and Rh,[105] given that these metals form three-dimensional clusters even at low coverages, and the clusters prefer to reside at the energetically favored step sites. The growth of Mo[41] and Re[42] on $TiO_2(110)$ is more similar to that of Sn since high cluster densities and two-dimensional islands that nucleate uniformly across the surface are observed in all cases. Co on $TiO_2(110)$[47,112] exhibits intermediate behavior in the sense that three-dimensional clusters are formed, but there is no preference for clusters to be found at the step edges. Furthermore, Co,[47] Mo,[41] and Re[42] are oxophilic metals that reduce the titania support upon deposition at room temperature, and XPS experiments suggest that admetal oxides are formed, as also observed for Sn deposition. DFT calculations show that Sn atoms prefer to exist as small clusters rather than aggregating into larger islands due to both the strong Sn−TiO_2 interactions compared with Sn−Sn, and the charge transfer that leads to repulsive dipole interactions between Sn atoms. In contrast, for Pt, Au, Ni, and Co, the weaker admetal−TiO_2 interactions compared to admetal−admetal leads to the formation of larger three-dimensional clusters.

The deposition of Pt on the existing Sn/SnO_x clusters results in exclusively bimetallic clusters since all Pt atoms are incorporated into the existing clusters, and no new clusters are formed. The Pt on Sn clusters produced from equal coverages (0.13 ML) of Pt and Sn have surfaces that are Sn-rich, which indicates high mobility of atoms within the clusters based on the ability of the Sn atoms to diffuse to the surface. Moreover, the addition of Pt to the existing clusters causes the decomposition of SnO_x, as demonstrated by both the experiment and theory; this behavior is attributed to the energetically favorable formation of Pt−Sn bonds that result in diffusion of Sn away from the cluster−support interface. Decomposition of Sn oxide that is thermodynamically driven by PtSn alloy formation was also reported for PtSn clusters on ceria thin films.[113] In this work from the Libuda group, ceria was initially doped with Sn^{4+} by deposition of metallic Sn, which was oxidized by lattice oxygen from the ceria support; subsequent deposition of Pt onto this surface resulted in alloying with Pt and reduction of Sn to the metallic state. For the Sn clusters deposited onto the existing Pt clusters on TiO_2 studied here, two scenarios are observed: Sn atoms are incorporated into Pt clusters to form PtSn alloys and SnO_x clusters nucleate on the surface, illustrating the short diffusion length for Sn atoms compared to Pt. Small positive shifts in the $Sn(3d_{5/2})$ and $Pt(4f_{7/2})$ binding energies for the bimetallic clusters compared to the monometallic clusters are consistent with PtSn alloy formation, although the shift in the $Pt(4f_{7/2})$ peak could also be attributed in part to the surface core level shift that occurs when surface Pt atoms are covered by Sn. The observed alloying of Pt and Sn is not surprising, given that PtSn alloys are formed over a wide compositional range and are thermodynamically favored over segregated Pt and Sn phases.[87]

The strong interaction between deposited Sn and the $TiO_2(110)$ support is consistent with the formation of a Sn−Ti−O alloy, particularly after the surface is heated to higher temperatures during the sputtering/annealing process to remove Sn. Sn is difficult to remove from the surface and requires ~15 sputtering/annealing cycles to remove 0.05−0.13 ML Sn. Specifically, STM imaging shows that small clusters (2−3 Å in height) remain on the surface after many cleaning cycles, and the number of these clusters tends to increase with increasing Sn coverage. The TiO_2 crystal also becomes more reduced over time after Sn deposition. Notably, the identical rutile structures of SnO_2 and TiO_2 as well as the similar ionic radii for Sn^{4+} and Ti^{4+} result in Sn^{4+} being readily substituted for Ti^{4+}.[8,18] Furthermore, deposition of metallic Sn on TiO_2 has also resulted in the formation of stable solid solutions over a large compositional range.[18,97,114−118]

■ CONCLUSIONS

The deposition of low coverages on Sn on $TiO_2(110)$ results in small, single-layer high clusters of SnO_x. At higher coverages, three-dimensional clusters containing metallic Sn are formed, but SnO_x still exists at the interface between the cluster and the TiO_2 support. DFT calculations demonstrate that Sn−Sn interactions are weaker than Sn−TiO_2 interactions, and there are repulsive dipole−dipole forces between Sn atoms; these results are consistent with the tendency of Sn to form small clusters on TiO_2, while other transition metals such as Pt, which has stronger metal−metal interactions, tend to agglomerate. The deposition of Pt on the existing Sn/SnO_x clusters produces exclusively bimetallic clusters, but the addition of Pt diminishes the amount of oxidized Sn. DFT investigations confirm that the formation of strong Pt−Sn bonds weakens the Sn−O interactions, allowing the Sn atoms at the interface to diffuse into the cluster and alloy with the Pt atoms.

■ ASSOCIATED CONTENT

Supporting Information

The Supporting Information is available free of charge at https://pubs.acs.org/doi/10.1021/acs.jpcc.1c03338.

> Cluster height histograms for 0.02 and 0.25 ML Sn; Pt(4f), Ti(2p), and O(1s) XPS data for pure Pt and Pt−Sn clusters; TiO_2 slab structures, cluster geometries, and binding sites used in DFT calculations; and per atom binding energies calculated by DFT for isolated atoms and clusters (PDF)

■ AUTHOR INFORMATION

Corresponding Authors

Graeme Henkelman − *Department of Chemistry and the Oden Institute for Computational and Engineering Sciences, University of Texas, Austin, Texas 78712, United States;* Phone: 803-777-1050; Email: dachen@sc.edu; Fax: 803-777-9521

Donna A. Chen − *Department of Chemistry and Biochemistry, University of South Carolina, Columbia, South Carolina 29208, United States;* orcid.org/0000-0003-4962-5530; Phone: 512-471-4179; Email: henkelman@utexas.edu

Authors

Sumit Beniwal − *Department of Chemistry and Biochemistry, University of South Carolina, Columbia, South Carolina 29208, United States*

Wenrui Chai − *Department of Chemistry and the Oden Institute for Computational and Engineering Sciences, University of Texas, Austin, Texas 78712, United States;* orcid.org/0000-0002-5801-0135

Kamolrat Metavarayuth − *Department of Chemistry and Biochemistry, University of South Carolina, Columbia, South Carolina 29208, United States;* Present Address: Ingevity, 5255 Virginia Avenue, North Charleston, SC 29206

Thathsara D. Maddumapatabandi − *Department of Chemistry and Biochemistry, University of South Carolina, Columbia, South Carolina 29208, United States;* Present Address: Sri Lanka Technology Campus, Ingiriya Road, Padukka, Sri Lanka

Deependra M. Shakya − *Department of Chemistry and Biochemistry, University of South Carolina, Columbia, South Carolina 29208, United States*

Complete contact information is available at: https://pubs.acs.org/10.1021/acs.jpcc.1c03338

Author Contributions

⊥S.B. and W.C. equally contributed to this work.

Notes

The authors declare no competing financial interest.

■ ACKNOWLEDGMENTS

We gratefully acknowledge financial support from the National Science Foundation (CHE 1764164); G.H. acknowledges the Welch Foundation (F-1841) and computational resources at the Texas Advanced Computing Center. We also thank Kihyun Shin for valuable scientific discussions.

■ REFERENCES

(1) Huidobro, A.; Sepúlveda-Escribano, A.; Rodríguez-Reinoso, F. Vapor-Phase Hydrogenation of Crotonaldehyde on Titania-Supported Pt and PtSn SMSI Catalysts. *J. Catal.* **2002**, *212*, 94−103.

(2) Altmann, L.; Wang, X.; Borchert, H.; Kolny-Olesiak, J.; Zielasek, V.; Parisi, J.; Kunz, S.; Bäumer, M. Influence of Sn Content on the Hydrogenation of Crotonaldehyde Catalysed by Colloidally Prepared PtSn Nanoparticles. *Phys. Chem. Chem. Phys.* **2015**, *17*, 28186−28192.

(3) Carney, C. M.; Yoo, S.; Akbar, S. A. TiO_2-SnO_2 Nanostructures and Their H_2 Sensing Behavior. *Sens. Actuators, B* **2005**, *108*, 29−33.

(4) Palgrave, R. G.; Bourlange, A.; Payne, D. J.; S. Foord, J.; Egdell, R. G. Interfacial Diffusion During Growth of $SnO_2(110)$ on $TiO_2(110)$ by Oxygen Plasma Assisted Molecular Beam Epitaxy. *Cryst. Growth Des.* **2009**, *9*, 1793−1797.

(5) Lübke, M.; Johnson, I.; Makwana, N. M.; Brett, D.; Shearing, P.; Liu, Z.; Darr, J. A. High Power TiO_2 and High Capacity Sn-doped TiO_2 Nanomaterial Anodes for Lithium-Ion Batteries. *J. Power Sources* **2015**, *294*, 94−102.

(6) Li, Y.; Zhu, S.; Inoue, A.; Liang, Y.; Chang, C.; Luo, S.; Cui, Z. Preparation of Nanoporous Sn-doped TiO_2 Anode Material for Lithium-Ion Batteries by a Simple Dealloying Method. *Ionics* **2020**, *26*, 4363−4372.

(7) Lee, D.-K.; Kwon, S.-H.; Ahn, J.-H. Growth of Rutile-TiO_2 Thin Films Via Sn Doping and Insertion of Ultra-Thin SnO_2 Interlayer by Atomic Layer Deposition. *Mater. Lett.* **2019**, *246*, 1−4.

(8) Sambrano, J. R.; Nóbrega, G. F.; Taft, C. A.; Andrés, J.; Beltrán, A. A Theoretical Analysis of the TiO_2/Sn Doped (110) Surface Properties. *Surf. Sci.* **2005**, *580*, 71−79.

(9) Tian, Q.; Wei, W.; Dai, J.; Sun, Q.; Zhuang, J.; Zheng, Y.; Liu, P.; Fan, M.; Chen, L. Porous Core-Shell $Ti_xSn_{1-x}O_2$ Solid Solutions with Broad-Light Response: One-Pot Synthesis and Ultrahigh Photooxidation Performance. *Appl. Catal., B* **2019**, *244*, 45−55.

(10) Carotta, M. C.; Gherardi, S.; Guidi, V.; Malagù, C.; Martinelli, G.; Vendemiati, B.; Sacerdoti, M.; Ghiotti, G.; Morandi, S. Electrical and Spectroscopic Properties of $Ti_{0.2}Sn_{0.8}O_2$ Solid Solution for Gas Sensing. *Thin Solid Films* **2009**, *517*, 6176−6183.

(11) Zakrzewska, K.; Radecka, M.; Rekas, M. Effect of Nb, Cr, Sn Additions on Gas Sensing Properties of TiO_2 Thin Films. *Thin Solid Films* **1997**, *310*, 161−166.

(12) Tada, H.; Hattori, A.; Tokihisa, Y.; Imai, K.; Tohge, N.; Ito, S. A Patterned-TiO_2/SnO_2 Bilayer Type Photocatalyst. *J. Phys. Chem. B* **2000**, *104*, 4585−4587.

(13) Radecka, M.; Zakrzewska, K.; Rękas, M. SnO_2-TiO_2 Solid Solutions for Gas Sensors. *Sens. Actuators, B* **1998**, *47*, 194−204.

(14) Radecka, M.; Przewoźnik, J.; Zakrzewska, K. Microstructure and Gas-Sensing Properties of (Sn, Ti)O_2 Thin Films Deposited by Rgto Technique. *Thin Solid Films* **2001**, *391*, 247−254.

(15) Cao, Y.; Zhang, X.; Yang, W.; Du, H.; Bai, Y.; Li, T.; Yao, J. A Bicomponent TiO_2/SnO_2 Particulate Film for Photocatalysis. *Chem. Mat.* **2000**, *12*, 3445−3448.

(16) Wang, S.; Zhu, Y.; Liu, B.; Wang, C.; Ma, R. Enhanced Performance of Mesostructured Perovskite Solar Cells with a Composite Sn^{4+}-doped TiO_2 Electron Transport Layer. *Ionics* **2019**, *25*, 4509−4516.

(17) Solís-Casados, D. A.; Martínez-Peña, J.; Hernández-López, S.; Escobar-Alarcón, L. Photocatalytic Degradation of the Malachite Green Dye with Simulated Solar Light Using TiO_2 Modified with Sn and Eu. *Top. Catal.* **2020**, *63*, 564−574.

(18) Zhu, X.; Han, S.; Feng, W.; Kong, Q.; Dong, Z.; Wang, C.; Lei, J.; Yi, Q. The Effect of Heat Treatment on the Anatase-Rutile Phase Transformation and Photocatalytic Activity of Sn-doped TiO_2 Nanomaterials. *RSC Adv.* **2018**, *8*, 14249−14257.

(19) Themlin, J.-M.; Chtaïb, M.; Henrard, L.; Lambin, P.; Darville, J.; Gilles, J.-M. Characterization of Tin Oxides by X-Ray-Photoemission Spectroscopy. *Phys. Rev. B: Condens. Matter Mater. Phys.* **1992**, *46*, 2460−2466.

(20) Lin, J.; Yu, J. C.; Lo, D.; Lam, S. K. Photocatalytic Activity of Rutile $Ti_{1-x}Sn_xO_2$ Solid Solutions. *J. Catal.* **1999**, *183*, 368−372.

(21) Inomata, Y.; Albrecht, K.; Yamamoto, K. Size-Dependent Oxidation State and CO Oxidation Activity of Tin Oxide Clusters. *ACS Catal.* **2018**, *8*, 451−456.

(22) Deng, L.; Miura, H.; Shishido, T.; Wang, Z.; Hosokawa, S.; Teramura, K.; Tanaka, T. Elucidating Strong Metal-Support Interactions in Pt-Sn/SiO_2 Catalyst and Its Consequences for Dehydrogenation of Lower Alkanes. *J. Catal.* **2018**, *365*, 277−291.

(23) Srisakwattana, T.; Suriye, K.; Praserthdam, P.; Panpranot, J. Preparation of Aluminum Magnesium Oxide by Different Methods for Use as PtSn Catalyst Supports in Propane Dehydrogenation. *Catal. Today* **2020**, *358*, 90−99.

(24) Michalak, W. D.; Krier, J. M.; Alayoglu, S.; Shin, J.-Y.; An, K.; Komvopoulos, K.; Liu, Z.; Somorjai, G. A. CO Oxidation on PtSn Nanoparticle Catalysts Occurs at the Interface of Pt and Sn Oxide Domains Formed under Reaction Conditions. *J. Catal.* **2014**, *312*, 17−25.

(25) Rong, H.; Niu, Z.; Zhao, Y.; Cheng, H.; Li, Z.; Ma, L.; Li, J.; Wei, S.; Li, Y. Structure Evolution and Associated Catalytic Properties of PtSn Bimetallic Nanoparticles. *Chem.—Eur. J.* **2015**, *21*, 12034−12041.

(26) Marinelli, T. B. L. W.; Nabuurs, S.; Ponec, V. Activity and Selectivity in the Reactions of Substituted Alpha,Beta-Unsaturated Aldehydes. *J. Catal.* **1995**, *151*, 431−438.

(27) Coloma, F.; Sepúlveda-Escribano, A.; Fierro, J. L. G.; Rodríguez-Reinoso, F. Crotonaldehyde Hydrogenation over Bimetallic Pt-Sn Catalysts Supported on Pregraphitized Carbon Black. Effect of the Preparation Method. *Appl. Catal., A* **1996**, *148*, 63−80.

(28) Coloma, F.; Llorca, J.; Homs, N.; Ramírez de la Piscina, P.; Rodríguez-Reinoso, F.; Sepúlveda-Escribano, A. Crotonaldehyde Hydrogenation over Alumina- and Silica-Supported Pt-Sn Catalysts of Different Composition. In Situ DRIFT Study. *Phys. Chem. Chem. Phys.* **2000**, *2*, 3063−3069.

(29) Panja, C.; Saliba, N. A.; Koel, B. E. Coking Resistance of Pt-Sn Alloys Probed by Acetylene Chemisorption. *Catal. Lett.* **2000**, *68*, 175−180.

(30) Pham, H. N.; Sattler, J. J. H. B.; Weckhuysen, B. M.; Datye, A. K. Role of Sn in the Regeneration of Pt/Gamma-Al_2O_3 Light Alkane Dehydrogenation Catalysts. *ACS Catal.* **2016**, *6*, 2257−2264.

(31) Sattler, J. J. H. B.; Beale, A. M.; Weckhuysen, B. M. Operando Raman Spectroscopy Study on the Deactivation of Pt/Al_2O_3 and Pt-Sn/Al_2O_3 Propane Dehydrogenation Catalysts. *Phys. Chem. Chem. Phys.* **2013**, *15*, 12095−12103.

(32) Poondi, D.; Vannice, M. A. The Influence of MSI (Metal-Support Interactions) on Phenylacetaldehyde Hydrogenation over Pt Catalysts. *J. Mol. Catal. A: Chem.* **1997**, *124*, 79−89.

(33) Coloma, F.; Coronado, J. M.; Rochester, C. H.; Anderson, J. A. Infrared Study of Crotonaldehyde and CO Adsorption on a Pt/TiO_2 Catalyst. *Catal. Lett.* **1998**, *51*, 155−162.

(34) Dandekar, A.; Vannice, M. A. Crotonaldehyde Hydrogenation on Pt/TiO_2 and Ni/TiO_2 SMSI Catalysts. *J. Catal.* **1999**, *183*, 344−354.

(35) Vannice, M.; Sen, B. Metal Support Effects on the Intramolecular Selectivity of Crotonaldehyde Hydrogenation over Platinum. *J. Catal.* **1989**, *115*, 65−78.

(36) Stagg, S. M.; Querini, C. A.; Alvarez, W. E.; Resasco, D. E. Isobutane Dehydrogenation on Pt-Sn/SiO_2 Catalysts: Effect of Preparation Variables and Regeneration Treatments. *J. Catal.* **1997**, *168*, 75−94.

(37) Merlen, E.; Beccat, P.; Bertolini, J. C.; Delichère, P.; Zanier, N.; Didillon, B. Characterization of Bimetallic Pt-Sn/Al_2O_3 Catalysts: Relationship between Particle Size and Structure. *J. Catal.* **1996**, *159*, 178−188.

(38) Kuznetsov, V.; Belyi, A. S.; Yurchenko, E. N.; Smolikov, M. D.; Protasova, M. T.; Zatolokina, E. V.; Duplyakin, V. K. Mossbauer Spectroscopic and Chemical Analysis of the Composition of Sn-Containing Components of Pt-Sn/Al_2O_3 (CI) Reforming Catalyst. *J. Catal.* **1986**, *99*, 159−170.

(39) de Miguel, S. R.; Román-Martínez, M. C.; Jablonski, E. L.; Fierro, J. L. G.; Cazorla-Amorós, D.; Scelza, O. A. Characterization of Bimetallic PtSn Catalysts Supported on Purified and H_2O_2-Functionalized Carbons Used for Hydrogenation Reactions. *J. Catal.* **1999**, *184*, 514−525.

(40) Shi, L.; Deng, G.-M.; Li, W.-C.; Miao, S.; Wang, Q.-N.; Zhang, W.-P.; Lu, A.-H. Al_2O_3 Nanosheets Rich in Pentacoordinate Al^{3+} Ions Stabilize Pt-Sn Clusters for Propane Dehydrogenation. *Angew. Chem.* **2015**, *54*, 13994−13998.

(41) Galhenage, R. P.; Yan, H.; Rawal, T. B.; Le, D.; Brandt, A. J.; Maddumapatabandi, T. D.; Nguyen, N.; Rahman, T. S.; Chen, D. A. MoS_2 Nanoclusters Grown on TiO_2 : Evidence for New Adsorption Sites at Edges and Sulfur Vacancies. *J. Phys. Chem. C* **2019**, *123*, 7185−7201.

(42) Galhenage, R. P.; Xie, K.; Yan, H.; Seuser, G. S.; Chen, D. A. Understanding the Growth, Chemical Activity, and Cluster-Support Interactions for Pt-Re Bimetallic Clusters on TiO_2(110). *J. Phys. Chem. C* **2016**, *120*, 10866−10878.

(43) Duke, A. S.; Xie, K.; Brandt, A. J.; Maddumapatabandi, T. D.; Ammal, S. C.; Heyden, A.; Monnier, J. R.; Chen, D. A. Understanding Active Sites in the Water-Gas Shift Reaction for Pt-Re Catalysts on Titania. *ACS Catal.* **2017**, *7*, 2597−2606.

(44) Duke, A. S.; Xie, K.; Monnier, J. R.; Chen, D. A. Superior Long-Term Activity for a Pt-Re Alloy Compared to Pt in Methanol Oxidation Reactions. *Surf. Sci.* **2017**, *657*, 35−43.

(45) Brandt, A. J.; Maddumapatabandi, T. D.; Shakya, D. M.; Xie, K.; Seuser, G. S.; Farzandh, S.; Chen, D. A. Water-Gas Shift Activity on Pt-Re Surfaces and the Role of the Support. *J. Chem. Phys.* **2019**, *151*, 234714.

(46) Park, J. B.; Ratliff, J. S.; Ma, S.; Chen, D. A. Understanding the Reactivity of Oxide-Supported Bimetallic Clusters: Reaction of NO with CO on TiO_2(110)-Supported Pt-Rh Clusters. *J. Phys. Chem. C* **2007**, *111*, 2165−2176.

(47) Galhenage, R. P.; Ammal, S. C.; Yan, H.; Duke, A. S.; Tenney, S. A.; Heyden, A.; Chen, D. A. Nucleation, Growth and Adsorbate-Induced Changes in Composition for Co-Au Bimetallic Clusters on TiO_2. *J. Phys. Chem. C* **2012**, *116*, 24616−24629.

(48) Tenney, S. A.; He, W.; Roberts, C. C.; Ratliff, J. S.; Shah, S. I.; Shafai, G. S.; Turkowski, V.; Rahman, T. S.; Chen, D. A. CO-Induced Diffusion of Ni Atoms to the Surface of Ni−Au Clusters on TiO_2(110). *J. Phys. Chem. C* **2011**, *115*, 11112−11123.

(49) Ratliff, J. S. The Morphology and Catalytic Activity of Bimetallic Nanoclusters Supported on TiO_2(110). Ph.D. Thesis, University of South Carolina, Columbia, SC, 2009.

(50) Park, J. B.; Conner, S. F.; Chen, D. A. Bimetallic Pt-Au Clusters on TiO_2(110): Growth, Surface Composition and Metal-Support Interactions. *J. Phys. Chem. C* **2008**, *112*, 5490−5500.

(51) Stempel, S.; Bäumer, M.; Freund, H.-J. STM Studies of Rhodium Deposits on an Ordered Alumina Film - Resolution and Tip Effects. *Surf. Sci.* **1998**, *402–404*, 424–427.

(52) Horcas, I.; Fernandez, R.; Gómez-Rodríguez, J. M.; Colchero, J.; Gómez-Herrero, J.; Baro, A. M. WSXM: A Software for Scanning Probe Microscopy and a Tool for Nanotechnology. *Rev. Sci. Instrum.* **2007**, *78*, 013705.

(53) *Practical Surface Analysis: By Auger and X-ray Photoelectron Spectroscopy*; Briggs, D., Seah, M. P., Eds.; John Wiley and Sons, Inc.: Chichester, U.K., 1983.

(54) Jerdev, D. I.; Koel, B. E. Oxidation of Ordered Pt-Sn Surface Alloys by O_2. *Surf. Sci.* **2001**, *492*, 106–114.

(55) Axnanda, S.; Zhu, Z.; Zhou, W.; Mao, B.; Chang, R.; Rani, S.; Crumlin, E.; Somorjai, G.; Liu, Z. In Situ Characterizations of Nanostructured SnO_x/Pt(111) Surfaces Using Ambient-Pressure XPS (APXPS) and High-Pressure Scanning Tunneling Microscopy (HPSTM). *J. Phys. Chem. C* **2014**, *118*, 1935–1943.

(56) Axnanda, S.; Zhou, W.-P.; White, M. G. CO Oxidation on Nanostructured SnO_x/Pt(111) Surfaces: Unique Properties of Reduced SnO_x. *Phys. Chem. Chem. Phys.* **2012**, *14*, 10207–10214.

(57) Bullock, E. L.; Patthey, L.; Steinemann, S. G. Clean and Hydroxylated Rutile TiO_2(110) Surfaces Studied by X-ray Photoelectron Spectroscopy. *Surf. Sci.* **1996**, *352–354*, 504–510.

(58) Dupin, J.-C.; Gonbeau, D.; Vinatier, P.; Levasseur, A. Systematic XPS Studies of Metal Oxides, Hydroxides and Peroxides. *Phys. Chem. Chem. Phys.* **2000**, *2*, 1319–1324.

(59) Jugnet, Y.; Loffreda, D.; Dupont, C.; Delbecq, F.; Ehret, E.; Cadete Santos Aires, F. J.; Mun, B. S.; Aksoy Akgul, F.; Liu, Z. Promoter Effect of Early Stage Grown Surface Oxides: A Near Ambient-Pressure XPS Study of CO Oxidation on PtSn Bimetallics. *J. Phys. Chem. Lett.* **2012**, *3*, 3707–3714.

(60) Kresse, G.; Hafner, J. Ab Initio Molecular-Dynamics for Liquid-Metals. *Phys. Rev. B: Condens. Matter Mater. Phys.* **1993**, *47*, 558–561.

(61) Kresse, G.; Furthmüller, J. Efficiency of Ab-Initio Total Energy Calculations for Metals and Semiconductors Using a Plane-Wave Basis Set. *Comput. Mater. Sci.* **1996**, *6*, 15–50.

(62) Kresse, G.; Furthmüller, J. Efficient Iterative Schemes for Ab Initio Total-Energy Calculations Using a Plane-Wave Basis Set. *Phys. Rev. B: Condens. Matter Mater. Phys.* **1996**, *54*, 11169–11186.

(63) Kresse, G.; Joubert, D. From Ultrasoft Pseudopotentials to the Projector Augmented-Wave Method. *Phys. Rev. B: Condens. Matter Mater. Phys.* **1999**, *59*, 1758–1775.

(64) Blöchl, P. E. Projector Augmented-Wave Method. *Phys. Rev. B: Condens. Matter Mater. Phys.* **1994**, *50*, 17953–17979.

(65) Perdew, J. P.; Burke, K.; Ernzerhof, M. Generalized Gradient Approximation Made Simple. *Phys. Rev. Lett.* **1996**, *77*, 3865–3868.

(66) Rice, C. M.; Eppelsheimer, D. S.; McNeil, M. B. Surface Tension of Solid Tin. *J. Appl. Phys.* **1966**, *37*, 4766–4768.

(67) *Cohesion in Metals: Transition Metal Alloys*; de Boer, F. R., Boom, R., Mattens, W. C. M., Miedema, A. R., Niessen, A. K., Eds.; North-Holland Physics Publishing: Amsterdam, 1998; Vol. *1*.

(68) Ramallo-López, J. M.; Santori, G. F.; Giovanetti, L.; Casella, M. L.; Ferretti, O. A.; Requejo, F. G. XPS and XAFS Pt L_2, L_3-Edge Studies of Dispersed Metallic Pt and PtSn Clusters on SiO_2 Obtained by Organometallic Synthesis: Structural and Electronic Characteristics. *J. Phys. Chem. B* **2003**, *107*, 11441–11451.

(69) Meitzner, G.; Via, G. H.; Lytle, F. W.; Fung, S. C.; Sinfelt, J. H. Extended X-Ray Absorption Fine-Structure Studies of Platinum Tin Catalysts. *J. Phys. Chem.* **1988**, *92*, 2925–2932.

(70) Tenney, S. A.; Ratliff, J. S.; Roberts, C. C.; He, W.; Ammal, S. C.; Heyden, A.; Chen, D. A. Adsorbate-Induced Changes in the Surface Composition of Bimetallic Clusters: Au-Pt on TiO_2(110). *J. Phys. Chem. C* **2010**, *114*, 21652–21663.

(71) Wagner, C. D.; Riggs, W. M.; Davis, L. E.; Moulder, J. F. *Handbook of X-ray Photoelectron Spectroscopy*; PerkinElmer Corporation: Eden Prairie, MN, 1979.

(72) Leiko, O.; Kosto, Y.; Mašek, K. Structural and Photoelectron Studies of Sn-SnO_x and SnO_2 Nanoparticles on TiO_2(110) Surface. *Surf. Interface Anal.* **2018**, *50*, 1116–1121.

(73) Rizo, R.; Arán-Ais, R. M.; Padgett, E.; Muller, D. A.; Lázaro, M. J.; Solla-Gullón, J.; Feliu, J. M.; Pastor, E.; Abruña, H. D. Pt-Rich$_{\text{core}}$/Sn-Rich$_{\text{subsurface}}$/Pt$_{\text{skin}}$ Nanocubes as Highly Active and Stable Electrocatalysts for the Ethanol Oxidation Reaction. *J. Am. Chem. Soc.* **2018**, *140*, 3791–3797.

(74) Godoi, D. R. M.; Perez, J.; Villullas, H. M. Alloys and Oxides on Carbon-Supported Pt-Sn Electrocatalysts for Ethanol Oxidation. *J. Power Sources* **2010**, *195*, 3394–3401.

(75) Kaylor, N.; Davis, R. J. Propane Dehydrogenation over Supported Pt-Sn Nanoparticles. *J. Catal.* **2018**, *367*, 181–193.

(76) Batzill, M.; Kim, J.; Beck, D. E.; Koel, B. E. Epitaxial Growth of Tin Oxide on Pt(111): Structure and Properties of Wetting Layers and SnO_2 Crystallites. *Phys. Rev. B: Condens. Matter Mater. Phys.* **2004**, *69*, 165403.

(77) Paál, Z.; Wootsch, A.; Teschner, D.; Lázár, K.; Sajó, I. E.; Győrffy, N.; Weinberg, G.; Knop-Gericke, A.; Schlögl, R. Structural Properties of an Unsupported Model Pt-Sn Catalyst and Its Catalytic Properties in Cyclohexene Transformation. *Appl. Catal., A* **2011**, *391*, 377–385.

(78) Lee, J. K.; Kim, Y.-K.; Choi, B. J.; Chung, T.-M.; Han, J. H. SnO-decorated TiO_2 Nanoparticle with Enhanced Photocatalytic Performance for Methylene Blue Degradation. *Appl. Surf. Sci.* **2019**, *480*, 1089–1092.

(79) Lau, C. L.; Wertheim, G. K. Oxidation of Tin : An ESCA Study. *J. Vac. Sci. Technol.* **1978**, *15*, 622–624.

(80) Hishita, S.; Janeček, P.; Haneda, H. Epitaxial Growth of Tin Oxide Film on TiO_2(110) Using Molecular Beam Epitaxy. *J. Cryst. Growth* **2010**, *312*, 3046–3049.

(81) Wang, X.; Stöver, J.; Zielasek, V.; Altmann, L.; Thiel, K.; Al-Shamery, K.; Bäumer, M.; Borchert, H.; Parisi, J.; Kolny-Olesiak, J. Colloidal Synthesis and Structural Control of PtSn Bimetallic Nanoparticles. *Langmuir* **2011**, *27*, 11052–11061.

(82) Paffett, M. T.; Windham, R. G. Surface Modification of Pt(111) by Sn Adatoms: Evidence for the Formation of Ordered Overlayers and Surface Alloys. *Surf. Sci.* **1989**, *208*, 34–54.

(83) Galeotti, M.; Atrei, A.; Bardi, U.; Rovida, G.; Torrini, M. Surface Alloying at the Sn-Pt(111) Interface: A Study by X-Ray Photoelectron Diffraction. *Surf. Sci.* **1994**, *313*, 349–354.

(84) Neitzel, A.; Kovács, G.; Lykhach, Y.; Kozlov, S. M.; Tsud, N.; Skála, T.; Vorokhta, M.; Matolín, V.; Neyman, K. M.; Libuda, J. Atomic Ordering and Sn Segregation in Pt-Sn Nanoalloys Supported on CeO_2 Thin Films. *Top. Catal.* **2017**, *60*, 522–532.

(85) Neitzel, A.; Kovács, G.; Lykhach, Y.; Tsud, N.; Kozlov, S. M.; Skála, T.; Vorokhta, M.; Matolín, V.; Neyman, K. M.; Libuda, J. Steering the Formation of Supported Pt-Sn Nanoalloys by Reactive Metal-Oxide Interaction. *RSC Adv.* **2016**, *6*, 85688–85697.

(86) Zhou, W.; Liu, L.; Li, B.; Wu, P.; Song, Q. Structural, Elastic and Electronic Properties of Intermetallics in the Pt-Sn System: A Density Functional Investigation. *Comput. Mater. Sci.* **2009**, *46*, 921–931.

(87) DeSario, D. Y.; DiSalvo, F. J. Ordered Intermetallic Pt-Sn Nanoparticles: Exploring Ordering Behavior across the Bulk Phase Diagram. *Chem. Mat.* **2014**, *26*, 2750–2757.

(88) Ramstad, A.; Strisland, F.; Raaen, S.; Worren, T.; Borg, A.; Berg, C. Growth and Alloy Formation Studied by Photoelectron Spectroscopy and STM. *Surf. Sci.* **1999**, *425*, 57–67.

(89) Björneholm, O.; Nilsson, A.; Tillborg, H.; Bennich, P.; Sandell, A.; Hernnäs, B.; Puglia, C.; Mårtensson, N. Overlayer Structure from Adsorbate and Substrate Core Level Binding Energy Shifts: CO, CCH_3, and O on Pt(111). *Surf. Sci.* **1994**, *315*, L983–L989.

(90) Singh, J.; Nelson, R. C.; Vicente, B. C.; Scott, S. L.; van Bokhoven, J. A. Electronic Structure of Alumina-Supported Monometallic Pt and Bimetallic PtSn Catalysts under Hydrogen and Carbon Monoxide Environment. *Phys. Chem. Chem. Phys.* **2010**, *12*, 5668–5677.

(91) Cheung, T. T. P. X-Ray Photoemission of Oxidized Sn-Pt and Pb-Pt Composites. *Surf. Sci.* **1986**, *177*, L887–L895.

(92) Altmann, L.; Wang, X.; Stöver, J.; Klink, M.; Zielasek, V.; Thiel, K.; Kolny-Olesiak, J.; Al-Shamery, K.; Borchert, H.; Parisi, J.; et al.

Impact of Organic Ligands on the Structure and Hydrogenation Performance of Colloidally Prepared Bimetallic PtSn Nanoparticles. *ChemCatChem* **2013**, *5*, 1803−1810.

(93) Diebold, U. The Surface Science of Titanium Dioxide. *Surf. Sci. Rep.* **2003**, *48*, 53−229.

(94) Mayer, J. T.; Diebold, U.; Madey, T. E.; Garfunkel, E. Titanium and Reduced Titania Overlayers on Titanium Dioxide(110). *J. Electron Spectrosc.* **1995**, *73*, 1−11.

(95) Göpel, W.; Anderson, J. A.; Frankel, D.; Jaehnig, M.; Phillips, K.; Schäfer, J. A.; Rocker, G. Surface-Defects of TiO_2(110): A Combined XPS, XAES and ELS Study. *Surf. Sci.* **1984**, *139*, 333−346.

(96) Sham, T. K.; Lazarus, M. S. X-Ray Photoelectron-Spectroscopy (XPS) Studies of Clean and Hydrated TiO_2 (Rutile) Surfaces. *Chem. Phys. Lett.* **1979**, *68*, 426−432.

(97) Batzill, M.; Diebold, U. The Surface and Materials Science of Tin Oxide. *Prog. Surf. Sci.* **2005**, *79*, 47−154.

(98) Jiménez, V. M.; Mejías, J. A.; Espinós, J. P.; González-Elipe, A. R. Interface Effects for Metal Oxide Thin Films Deposited on Another Metal Oxide II. SnO_2 Deposited on SiO_2. *Surf. Sci.* **1996**, *366*, 545−555.

(99) Gálvez-López, M. F.; Muñoz-Batista, M. J.; Alvarado-Beltrán, C. G.; Almaral-Sánchez, J. L.; Bachiller-Baeza, B.; Kubacka, A.; Fernández-García, M. Sn Modification of TiO_2 Anatase and Rutile Type Phases: 2-Propanol Photo-Oxidation under UV and Visible Light. *Appl. Catal., B* **2018**, *228*, 130−141.

(100) Henkelman, G.; Arnaldsson, A.; Jónsson, H. A Fast and Robust Algorithm for Bader Decomposition of Charge Density. *Comput. Mater. Sci.* **2006**, *36*, 354−360.

(101) Sanville, E.; Kenny, S. D.; Smith, R.; Henkelman, G. Improved Grid-Based Algorithm for Bader Charge Allocation. *J. Comput. Chem.* **2007**, *28*, 899−908.

(102) Tang, W.; Sanville, E.; Henkelman, G. A Grid-Based Bader Analysis Algorithm without Lattice Bias. *J. Phys.: Condens. Matter* **2009**, *21*, 084204.

(103) Eckardt, I.; Schröter, T.; Tiedtke, K.; Wagner, N. Photoemission Studies of Ultrathin Sn-Layers on TiO_{2-X} (Rutile). *Cryst. Res. Technol.* **1998**, *33*, 129−133.

(104) Fujitani, T.; Nakamura, J. The Chemical Modification Seen in the Cu/ZnO Methanol Synthesis Catalysts. *Appl. Catal., A* **2000**, *191*, 111−129.

(105) Park, J. B.; Ratliff, J. S.; Ma, S.; Chen, D. A. *In Situ* Scanning Tunneling Microscopy Studies of Bimetallic Cluster Growth: Pt-Rh on TiO_2(110). *Surf. Sci.* **2006**, *600*, 2913−2923.

(106) Zhou, J.; Kang, Y. C.; Chen, D. A. Controlling Island Size Distributions: A Comparison of Nickel and Copper Growth on TiO_2(110). *Surf. Sci.* **2003**, *537*, L429−L434.

(107) Wahlström, E.; Lopez, N.; Schaub, R.; Thostrup, P.; Rønnau, A.; Africh, C.; Laegsgaard, E.; Nørskov, J. K.; Besenbacher, F. Bonding of Gold Nanoclusters to Oxygen Vacancies on Rutile TiO_2(110). *Phys. Rev. Lett.* **2003**, *90*, 026101.

(108) Valden, M.; Lai, X.; Goodman, D. W. Onset of Catalytic Activity of Gold Clusters on Titania with the Appearance of Nonmetallic Properties. *Science* **1998**, *281*, 1647−1650.

(109) Jak, M. J. J.; Konstapel, C.; van Kreuningen, A.; Chrost, J.; Verhoeven, J.; Frenken, J. W. M. The Influence of Substrate Defects on the Growth Rate of Palladium Nanoparticles on a TiO_2(110) Surface. *Surf. Sci.* **2001**, *474*, 28−36.

(110) Chen, D. A.; Bartelt, M. C.; Hwang, R. Q.; McCarty, K. F. Self-Limiting Growth of Cu Islands on TiO_2(110). *Surf. Sci.* **2000**, *450*, 78−97.

(111) Chen, D. A.; Bartelt, M. C.; Seutter, S. M.; McCarty, K. F. Small, Uniform, and Thermally Stable Silver Particles on TiO_2(110)-(1x1). *Surf. Sci.* **2000**, *464*, L708−L714.

(112) Galhenage, R. P.; Yan, H.; Tenney, S. A.; Park, N.; Henkelman, G.; Albrecht, P.; Mullins, D. R.; Chen, D. A. Understanding the Nucleation and Growth of Metals on TiO_2: Co Compared to Au, Ni and Pt. *J. Phys. Chem. C* **2013**, *117*, 7191−7201.

(113) Neitzel, A.; Lykhach, Y.; Skála, T.; Tsud, N.; Johánek, V.; Vorokhta, M.; Prince, K. C.; Matolín, V.; Libuda, J. Hydrogen Activation on Pt-Sn Nanoalloys Supported on Mixed Sn-Ce Oxide Films. *Phys. Chem. Chem. Phys.* **2014**, *16*, 13209−13219.

(114) Mehraz, S.; Kongsong, P.; Taleb, A.; Dokhane, N.; Sikong, L. Large Scale and Facile Synthesis of Sn Doped TiO_2 Aggregates Using Hydrothermal Synthesis. *Sol. Energy Mater. Sol. Cells* **2019**, *189*, 254−262.

(115) Mahanty, S.; Roy, S.; Sen, S. Effect of Sn Doping on the Structural and Optical Properties of Sol-Gel TiO_2 Thin Films. *J. Cryst. Growth* **2004**, *261*, 77−81.

(116) Sayılkan, H. Improved Photocatalytic Activity of Sn^{4+}-doped and Undoped TiO_2 Thin Film Coated Stainless Steel under UV- and VIS-irradiation. *Appl. Catal., A* **2007**, *319*, 230−236.

(117) Sensato, F. R.; Custodio, R.; Longo, E.; Beltrán, A.; Andrés, J. Electronic and Structural Properties of $Sn_xTi_{1-x}O_2$ Solid Solutions: a Periodic DFT Study. *Catal. Today* **2003**, *85*, 145−152.

(118) Zakrzewska, K. Mixed Oxides as Gas Sensors. *Thin Solid Films* **2001**, *391*, 229−238.